ChemPlusChem

Research Article
doi.org/10.1002/cplu.202400408

Chemistry Europe
European Chemical Societies Publishing

www.chempluschem.org

Synthesis of Porous Carbon Honeycomb Structures Derived from Hemp for Hybrid Supercapacitors with Improved Electrochemistry

Manickam Minakshi,*[a] Agha Mujeeb,[a] Jonathan Whale,[a] Richard Evans,[b, c] Rob Aughterson,[d] Pragati A. Shinde,[e] Katsuhiko Ariga,[e, f] and Lok Kumar Shrestha*[e, g]

Energy storage in electrochemical hybrid capacitors involves fast faradaic reactions such as an intercalation, or redox process occurring at a solid electrode surface at an appropriate potential. Hybrid sodium-ion electrochemical capacitors bring the advantages of both the high specific power of capacitors and the high specific energy of batteries, where activated carbon serves as a critical electrode material. The charge storage in activated carbon arises from an adsorption process rather than a redox reaction and is an electrical double-layer capacitor. Advanced carbon materials with interconnecting porous structures possessing high surface area and high conductivity are the prerequisites 1128to qualify for efficient energy storage. Herein, we have demonstrated that a porous honeycomb structure activated carbon derived from Australian hemp hurd (*Cannabis sativa L.*) in aqueous Na_2SO_4 electrolyte showed a specific capacitance of 240 F/g at 1 A/g. The mass ratio of biochar to KOH during the chemical activation associated with the synthesis temperature influences the change in morphologies, and distribution of pore sizes on the adsorption of ions. At higher synthesis temperatures, the tubular form of the honeycomb starts to disintegrate. The hybrid sodium-ion device employing hemp-derived activated carbon (HAC) coupled with electrolytic manganese dioxide (EMD) in an aqueous Na_2SO_4 electrolyte showed a specific capacitance of 95 F/g at 1 A/g having a capacitance retention of 90%. The hybrid device (HAC||EMD) can possess excellent electrochemical performance metrics, having a high energy density of 38 Wh/kg at a power density of 761 W/kg. Overall, this study provides insights into the influence of the activation temperature and the KOH impregnation ratio on morphology, porosity distribution, and the activated carbon's electrochemical properties with faster kinetics. The high cell voltage for the device is devoted to the EMD electrode.

Introduction

Energy storage devices show great promise to meet the demands that the transition towards renewable energy sources and electrification of the transport sector put forward.[1] However, concerns regarding the current generation batteries include limited raw material resources and flammable electrolytes, necessitating research on alternative technologies. The organic electrolyte currently in use in lithium-ion batteries (LIBs) has several associated safety problems, including flammability and electrochemical instability.[2] Thus, it is important to choose safe electrolytes that have a very low reactivity towards the anode. From a safety perspective, aqueous electrolytes are the natural choice in this field.[3] Water is less expensive than organic solvents and has fewer disposal and safety issues. The ionic conductivity of aqueous electrolytes is two orders of magnitude greater than that of most organic electrolytes, allowing higher discharge rates and lower voltage drops due to electrolyte impedance. The main disadvantage of using an aqueous electrolyte is that the battery voltage is limited to ~2 V to avoid electrolysis.[3] To compensate for the effect of low voltage, the aqueous system's storage capacity and charge-

[a] *M. Minakshi, A. Mujeeb, J. Whale*
Engineering and Energy, Murdoch University, WA 6150, Australia
E-mail: minakshi@murdoch.edu.au

[b] *R. Evans*
Sustainable Futures, MIRRECO, Perth, WA 6000, Australia

[c] *R. Evans*
Sustainable Futures, MIRRECO®, Neptune Park, Plymouth, PL4 0SJ, England, UK

[d] *R. Aughterson*
Australian Nuclear Science and Technology Organization, NSW 2232, Australia

[e] *P. A. Shinde, K. Ariga, L. K. Shrestha*
Research Center for Materials Nanoarchitectonics (MANA), National Institute for Materials Science (NIMS), Tsukuba 305 0044, Japan
E-mail: SHRESTHA.Lokkumar@nims.go.jp

[f] *K. Ariga*
Department of Advanced Materials Science, Graduate School of Frontier Sciences, The University of Tokyo, 5–1–5 Kashiwanoha, Kashiwa, Chiba 277–8561, Japan

[g] *L. K. Shrestha*
Department of Materials Science, Institute of Pure and Applied Sciences, University of Tsukuba, 1–1, Tennodai, 305–8573 Tsukuba, Ibaraki, Japan

Supporting information for this article is available on the WWW under https://doi.org/10.1002/cplu.202400408

discharge characteristics must be significantly superior to those of non-aqueous systems. To meet prerequisites for high energy and high-power densities in a single application such as large-scale energy storage, devices that use sustainable materials must be developed with a combination of battery-type and capacitor-type materials.[4] In contrast to the poor power performance of LIBs, supercapacitors storing energy in an electric double layer (EDL) of electrolyte ions at the electrode surface can deliver high power density (pulse power) and a better life cycle.[4] Devices that can deliver both high power and energy density will meet a critical need in renewable energy technology. For such a purpose, it is crucial to improve the energy storage capability of the hybrid supercapacitors made by a combination of supercapacitor-type and battery-type electrode materials. Progress on the enhancement of energy density has been made in this work on the activated carbon electrode without sacrificing the power density in aqueous hybrid sodium-ion supercapacitors.

The strategic approach to improving the energy density of a hybrid sodium-ion system is to improve the specific capacitance of the electrode. Activated carbons (ACs) have played a significant role in the environmental, food, and pharmaceutical industries. The activated carbon derived from conventional non-renewable resources has a significant carbon footprint linked to their production. During the synthesis, a technology composed of carbonization and subsequent activation of carbon-rich precursors is traditionally used to prepare AC, which always requires a two-step calcination treatment at a high temperature of around 800 °C and increases its preparation cost for the storage device.[4–7] It is important to rethink the materials used in hybrid energy storage devices and studies are required to trial alternative sustainable materials. The characteristic of AC is the presence of surface functional groups, which are mainly present due to the physical/chemical activation processes that enhance the capacitance of AC.[8] On the other hand, the functional groups are claimed to be mainly responsible for storage performance degradation like inhibiting the rate capability.

Although a variety of AC materials possessing EDL behavior have been trialled in energy storage, this work takes the novel approach of using porous carbon derived from industrial hemp. The hemp-derived carbon (HAC) synthesized by a simple one-step with restricted functional groups, may produce an advanced storage material with higher performance. Commercially available activated carbon is relatively expensive and its cost stems from the chosen precursor, and methodology adopted to process the carbon. To reduce the cost of activated carbon, biomass as a precursor is receiving increased attention in recent times.[7,9,10] The activated carbon with various morphologies i.e. carbon fibers, carbon spheres, and carbon nanotubes has been reported from biomass precursors, which exhibit good electrochemical properties. Agricultural biomass is abundantly available and renewable, with higher lignocellulosic content. Additionally, the AC from biomass possesses a high surface area and a well-defined pore structure with enriched heteroatoms.[11] Hence, it is promising to use biomass in the form of industrial hemp, since it possesses inherent biodegradability and a good strength-to-weight ratio to produce low-cost AC.[12] For several years now, industrial hemp has been utilized across multiple civilizations and was grown to make the very first horseshoes, ropes, boat rigging, food, medicine, clothing, and construction markets. The last few years have since seen a leap in the use of industrial hemp in plastics, nutrition, health, protein, and composites.[11–13] With the natural world's strongest known fiber and unmatched carbon sequestration through ultra-fast growth and harvest, hemp is a very promising crop of the future. Industrial hemp (as shown in Figure 1) is an herbaceous and fast-growing annual crop that produces fiber and belongs to the Cannabis family. Only 25% of the hemp fibers from the fiber production process are useful and consequently, a high proportion of waste is produced. This waste, the lignified core tissue, shown in Figure 1, is referred to as "hemp hurd".[6] As the consumption of hemp is significantly high in the industries, the by-product must be disposed of efficiently. Therefore, repurposing the hemp hurd as a renewable energy resource could lead to a sustainable solution. The outer portion of the hemp hurd has a unique structure and connected pore geometry, which is a desirable characteristic for the adsorption of the obtained activated carbons. The activated carbon derived from hemp fiber can make a huge gain in solving the real challenge of aqueous batteries and super-

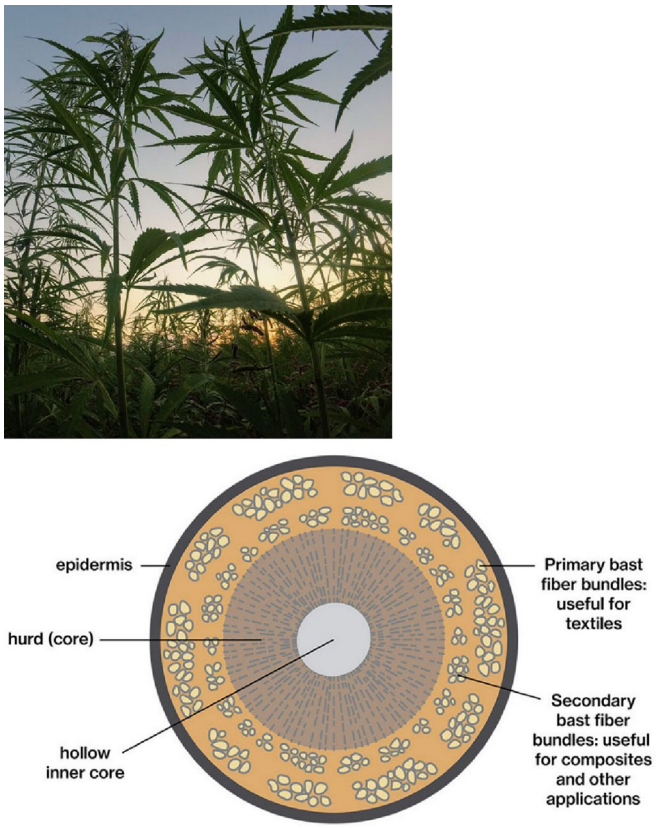

Figure 1. (left) Australian Industrial Hemp Hurd (Cannabis sativa L.), (right) Schematic representation of hemp cross-section. Adapted from Hemp Anatomy, 2024. Accessed 31/05/2024 https://wiki.opensourceecology.org/wiki/File:Hemp_stalk_anatomy.png.

capacitors, which lie at the interfaces between electrodes and electrolytes.[13]

In the proposed work, a novel approach to synthesize AC via one-step calcination of hemp stalk through the chemical activation agent potassium hydroxide (KOH) is postulated for hybrid capacitors with improved electrochemistry. The research uses industrial hemp produced in Western Australia (WA) with the constituents of hemp woody core (65%), in which cellulose is 40–48%, hemicellulose 18–24%; and lignin 21–23%, respectively; and hemp blast 35%, in which cellulose is 57–77%, hemicellulose 9–14%; and lignin 5–9%, respectively.[14] The homogenously mixed agricultural biomass hemp fiber powder with KOH solution plays the role of both a deoxidant and activating agent by skipping high-temperature synthesis in the conventional synthesis and this led to molecular level activation of hemp in subsequent one-step calcination of 450 °C. The formation of functional group challenges and requirements of high temperatures has been addressed here in a simple approach. The activated carbon derived from hemp fiber at optimum temperature is used as the electrode material with an electrolytic manganese dioxide (EMD) hybrid sodium-ion supercapacitor, and their electrochemical performance characteristics in aqueous Na_2SO_4 electrolytes are examined. The overall hybrid capacitor comprising HAC||EMD described in this work is found to have improved cell performance, energy density, and high-rate capability, which is attributed to the HAC electrode and the chosen electrolyte.

Results and Discussion

Physical Characterization of HAC

Structural (XRD)Analysis

The X-ray diffraction analyses were carried out on the hemp-derived activated carbon (HAC) prepared at different KOH impregnation ratios and mild to higher activation temperatures. In all the XRD patterns shown in Figure 2A, two broad peaks positioned around 22° and 43° were observed, corresponding to h k l Miller indices (002) and (100), respectively. This is as expected, and well-reported for other biomass-derived activated carbon.[6,15,16] The broadening of the observed two XRD peaks indicates the synthesized activated carbon is amorphous in nature. The shift of the (002) peak to lower 2θ values for a higher KOH impregnation ratio (1:2; carbon to KOH ratio) (Figure 2A) heated at both mild 450 °C (black curve) and higher 800 °C (green curve) activation temperatures indicates that the higher KOH increased the interlayer distance (d) between the graphitic sheets. The values of the interlayer distance are calculated using Bragg's law. The d_{002} values for the KOH impregnation ratio (1:1) is 3.53 Å, which increased to 4.05 and 4.1 Å for the higher KOH impregnation ratio (1:2) activated at mild, and higher temperatures, respectively. The obtained larger d-spacing of over 4.0 Å is classified as a highly disordered collection of small graphitic grains in the synthesized activated carbon. However, the position of the (100) peak remained

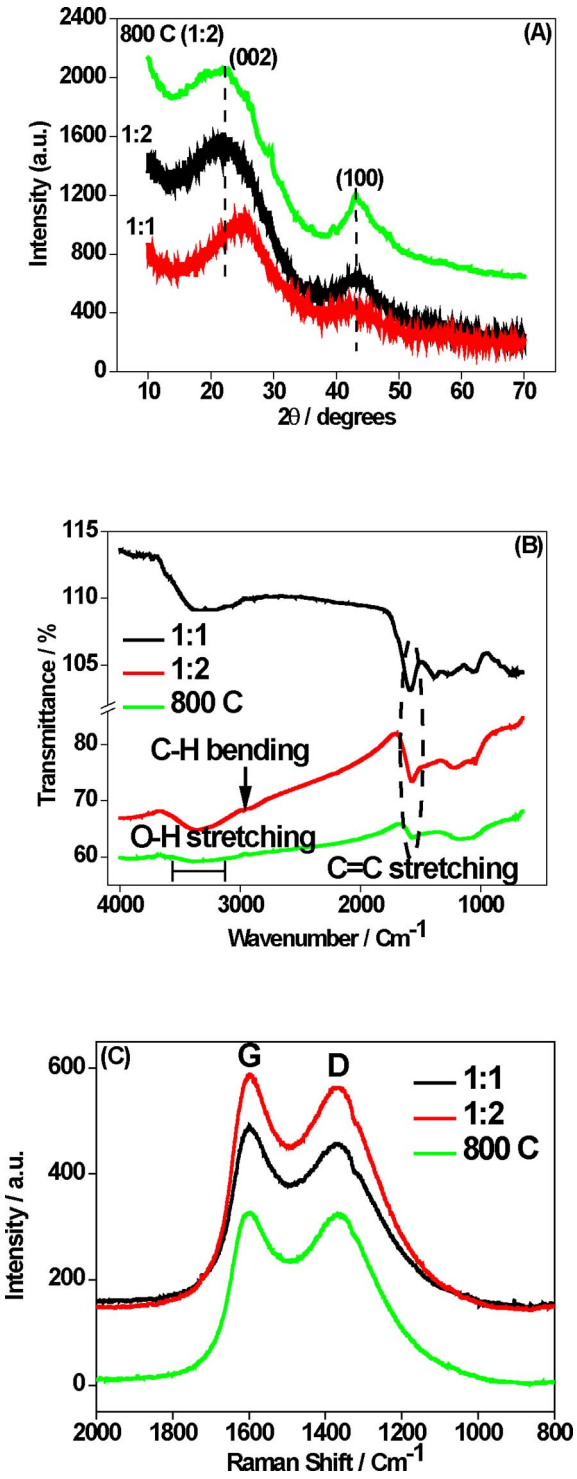

Figure 2. (a) X-ray diffraction patterns, (b) Mid and near infra-red (IR) spectra, and (c) Raman spectra of HAC. Samples are labeled in the individual plots.

constant with the d-spacing 2.1 Å. The hard carbons obtained at a higher d-spacing value could be suitable for use as an anode in sodium hybrid capacitors, which suits the size of the bigger ions like sodium. The average crystallite size was calculated using Scherrer's formula and found to be 1.3 nm. Overall, from the XRD analyses, it can be concluded that the

obtained interplanar spacing for amorphous hard carbon was significantly larger than that for the graphite anode (3.35 Å) indicating the suitability for a sodium hybrid device.[17] The more disordered structure is found for the impregnation ratio (1 : 2). The absence of any other secondary XRD peaks (like potassium) suggests that no impurities are present in the carbon produced from hemp-derived biomass.

Spectroscopy (FTIR and Raman) Analyses

The effect of activated carbon on the surface functional groups was studied by FTIR spectra and presented in Figure 2B. The spectra of the lower KOH impregnation ratio (1 : 1) showed an increase in intensities of three major adsorption bands at 1590 cm^{-1}, 2930 cm^{-1}, and 3360 cm^{-1}. The absorbance peak around 1590 cm^{-1} corresponds to C=C symmetrical stretching vibrations from the source lignin and is generally found in carbonaceous materials such as activated carbon,[14] and the peak around 2930 cm^{-1} corresponds to C–H bending in the rings and side groups of hemp.[18] The broadband near the IR region may be assigned to O–H stretching vibration due to intermolecular hydrogen bonding indicating the presence of free hydroxyl groups on the carbon surface.[19,20] Overall, the degree of deoxidation and hydroxylation bands at 1590 cm^{-1}, and the O–H group band at 3360 cm^{-1} derived from cellulose and hemicellulose in the hemp is decreased for the ratio (1 : 2) synthesized at 450 °C, and 800 °C in Figure 1B (curves a–b). The FTIR study concludes the presence of surface functional groups such as hydroxyl, and carboxy groups is lower in the activated carbon for the higher KOH impregnation ratio (1 : 2) activated at mild, and higher temperatures. Raman spectroscopy analysis was employed to further assess the structural disorder of the amorphous carbon. The two characteristic peaks observed (Figure 2C) at 1300 and 1600 cm^{-1} correspond to D (presence of disorder or defect in graphite) and G (degree of pure graphite) bands of sp^2 bonded carbon atoms, respectively.[6,19] The intensity ratio of D and G (I_D/I_G) for the samples is 0.95, 0.96. and 0.98 for the impregnation ratios (1 : 1), and (1 : 2) synthesized at 450 °C, and 800 °C, respectively. This shows the degree of structural disorder observed in the higher impregnation ratio is higher. It is expected that KOH activation disrupts the graphitic domain in a carbon matrix, resulting in a highly porous (as shown in the SEM images in the next section) with a disordered structure. However, at a higher activation temperature of 800 °C the melted KOH reacts with biochar, and with the insertion of K, the structure gets more disrupted.

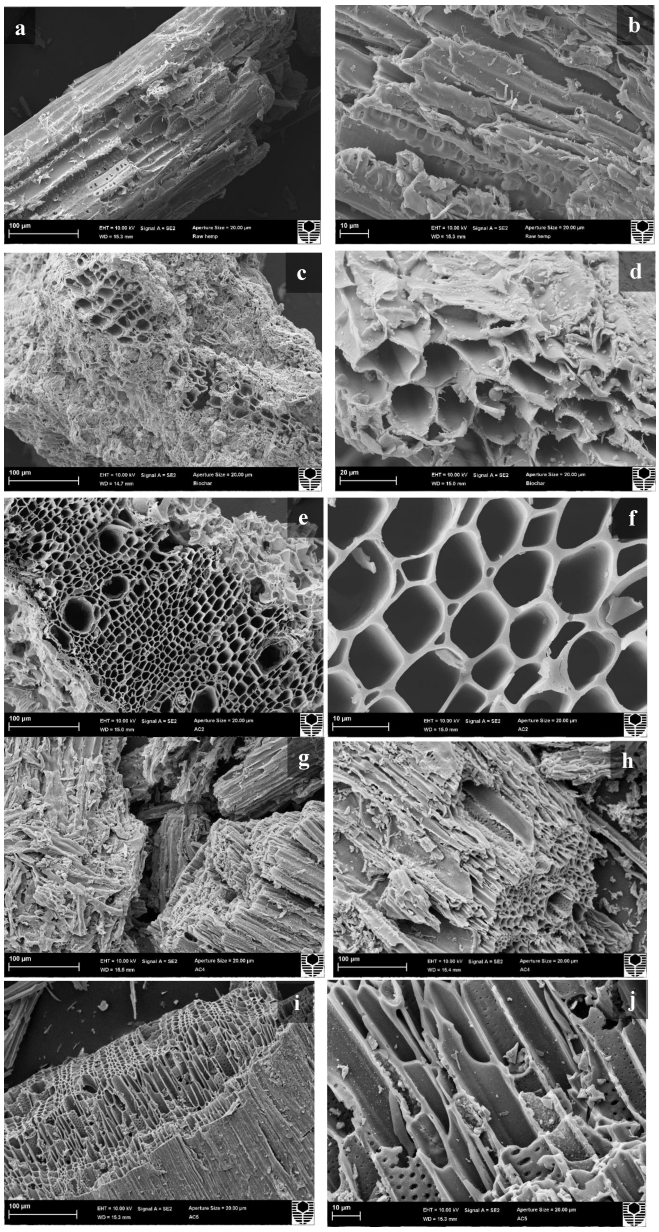

Figure 3. Scanning electron micrographs of the HAC under different conditions (a-b) long fiber structures of the raw hemp hurd, (c-d) biochar synthesized at 300 °C for 2 h showing porous tubular structure, (e-f) chemically activated carbons forms a structure with different morphologies at a mild temperature 450 °C for 1 h with mass ratios of KOH to biochar (1 : 1) having 3D honeycomb structure, (g-h) impregnation ratio (1 : 2) showing crystallites with compact porous turbostratic structure activated at 450 °C 1 h, (i-j) 1 : 2 activated at a higher temperature at 800 °C for 1 h showed disintegrated columns. The images on the left are at scales of 100 μm, and on the right are 10 μm.

Microscopy (SEM and STEM) Analyses

The morphological structure of hemp hurd was examined by SEM and STEM analyses. The SEM image of the raw hemp (seen in Figure 3a and b) exhibits a long hollow fiber structure, which is composed of cellulose, hemicellulose, and lignin.[21,22] The long fiber microscale structure of the raw hemp in the image Figure 3a and b shows vertical lines with grooves and pores in it.[22] These are beneficial for the adsorption of ions in the energy storage system. The morphologies of the carbonization of the raw hemp (defined as biochar) in Figure 3c and d show the decomposition of the fiber-like structure led to the evolution of a honeycomb-like structure having irregular microparticles ranging from 2–10 μm around the agglomerated layers of cellulosic particles. A fragment of brittle layers on a round-like pore channel with a diameter of around 5 μm is noted (in

Figure 3d), which could be a result of the ground tissues of the hemp. The pores in the carbonized hemp (biochar in Figure 3c and d) are well-connected and form more hollow structures. A similar microstructure has been reported for hemp shiv used for construction[23] but the pores are well below 1 μm in size found between cell wall layers. During the carbonization process, the decomposition of the lignin and hemicellulose decreases the material's crystallinity, as evidenced by the XRD in Figure 2A, and the dehydration creates a pore structure. Figure 3e and f shows the morphologies of the chemically activated carbon prepared at a lower impregnation ratio (1:1) activated at a mild temperature of 450 °C. The difference seen in the morphologies of the activated carbon (Figure 3e and f), and the biochar (in Figure 2c and d) indicates the chemical activation process can lead to the formation of a sturdy hierarchical porous 3D honeycomb structure with an increase in surface area to 1065 m^2/g. The elliptically wide pores ranging from 5–10 μm are shown in Figure 3e and f, which is spectacular and very different from the microstructure of hemp reported earlier.[24] Puangsin et al[24] displayed the microstructure of hemp, which is similar to the diffused porous wood. The authors[24] explain activation process can influence both the physicochemical and electrochemical properties of activated carbon electrodes significantly. To verify this, the impregnation ratio was increased to 1:2 and activated at different temperatures 450 and 800 °C, corresponding SEM images are shown in Figure 3g–j respectively. At a higher carbon to KOH ratio, Figure 3g and h, a compact porous turbostratic structure is evidenced with structural defects on the surface. This suggests that the surface area and pore volume of the mesopores and macropores are significantly higher than that of the biochar samples (see Table 1). The obtained surface area values and the pore size distribution of the activated carbon match well with the reported value.[25] The connected pore geometry with a high specific surface area, which is evenly distributed, may provide more attachment sites for sodium ions in the electrolyte. These observations are very unique, and to the best of our knowledge, no such unique microstructure of hierarchical porous structure has been demonstrated for energy storage applications. The reported SEM images for hemp as a precursor for obtaining activated carbon[6,13,19] are quite different from those reported in this work. While at a higher activation temperature (800 °C), the degradation of the hollow structure is evident from Figure 3i and j. This is shown by the Brunauer-Emmett-Teller (BET) surface area and the pore volume tabulated in Table 1, where the values are decreased compared to the lower temperature for the 1:2 ratio. This could be due to the higher degree of the insertion of melted potassium compound into the carbon structure and a few may be left unreacted. It could be concluded that the KOH impregnation ratio, and activation temperature influence morphology, the degree of disorder, and porosity distribution. Table 1 suggests the carbon to KOH ratio (1:2) activating at 450 °C with the highest surface area and pore volume, is the most feasible for supercapacitor applications. This approach of one-step activation at a mild temperature of 450 °C to obtain HAC appears to be not reported widely. The optimized disordered and graphitic interconnected porous turbostratic structure of the HAC (seen in Figure 3g and h) with well-arranged hierarchical porosity is expected to provide enhanced electrochemical capacitive properties in Na_2SO_4 electrolytes. The corresponding HRTEM image of the HAC sample in Figure S2 showed a highly amorphous structure with a color contrast that can be observed with highly disordered and curled carbon layers. The composition profile shows the carbon is well dispersed in the sampling.

Table 1. BET Surface area and pore volumes for the HAC obtained at different conditions

Sample	BET Surface Area (m^2/g)	Correlation Coeff	t-Pore Area (m^2/g)	t-PoreVolume (cm^3/g)
Biochar	2.32	0.9997	1.1169	0.00044
1:1 ratio	1065.74	0.9999	582.34	0.23966
1:2 ratio	1195.70	0.9999	820.48	0.33036
800 C (1:2)	907.11	0.999	656.06	0.26133

The STEM images of the hemp-derived carbon to KOH ratio (1:2) activating at mild 450 °C are shown in Figure 4a–c. The images in various areas of interest invariably show amorphous regions with columnar striations on the surface. Numerous micro-sized pores exist in the carbon backbone, confirming its well-developed hierarchical porous structure. Interestingly, the color-coded elemental mapping of the STEM analysis in the regions (example shown in Figure 4d) shows hemp plant is also seen to be a source of minerals such as phosphorous and calcium (in the form of calcium phosphate). This is not surprising, as Ca is reported to be found as one of the most abundant species in waste hemp products.[6] If the volume fraction of these elements is below the detection limit in bulk XRD then it will not be identified in the XRD crystal structure shown in Figure 2A. These elements played a key role in promoting devolatilization that led to morphological and structural disorders in the final product. Relatively thin carbon sheets with randomly oriented ordered domains with several other particles clinging on the surface are illustrated in Figure 4b and c. The compact tubular structure is viewed in Figure 4b. In the case of activating at higher 800 °C, (Figure 4e–h) distinguishable surface textures with different thicknesses are observed. As with the 450 °C specimen, STEM EDS mapping of the 800 °C specimen shows the presence of calcium phosphate inclusions (Figure 4e–f). The higher magnification bright field images for the 800 °C specimen (Figure 4g–h) highlight the porous nature of these specimens. The information extracted from the XRD, and spectroscopy analyses qualitatively agreed with the findings deduced from microscopy results. Therefore, the hemp-derived carbon with an impregnation ratio (1:2) activated at 450 °C has been tested for supercapacitor studies.

To study the chemical composition and surface properties of the HAC (1:2) activated at 450 °C sample, X-ray photoelectron spectroscopy (XPS) was carried out and the high-resolution C 1s and O 1s deconvoluted with other sub-peaks

Research Article
doi.org/10.1002/cplu.202400408

Chemistry Europe
European Chemical Societies Publishing

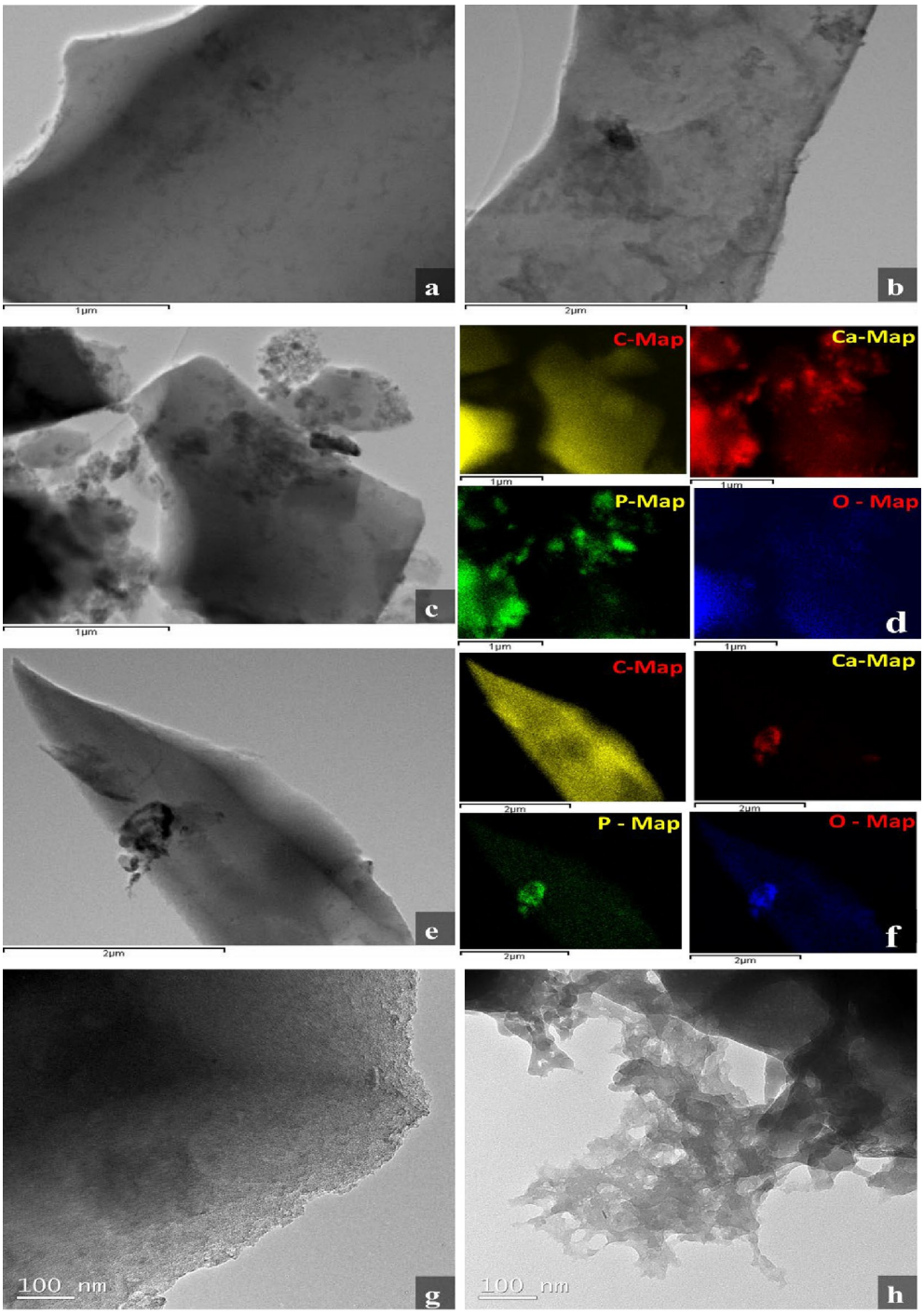

Figure 4. Transmission electron micrographs (TEM) of the HAC synthesized with mass ratios of biochar to KOH (1 : 2) (a–d) 450 °C, and (e–h) 800 °C for 1 hr. Images (a–c) are scanning TEM (STEM) images, with (d) showing corresponding X-ray energy dispersive spectroscopy (EDS) color-coded maps (carbon, calcium, phosphorus, and oxygen) from regions of interest in (c). STEM image (e) with corresponding EDS color-coded maps shown in (f). (g and h) show higher magnification of TEM bright field images.

are shown in Figure S1. The C 1s spectrum in Figure S1 is deconvoluted into three peaks at 285.15, 286.5, and 289.2 eV, which are ascribed to C=C, C–C, and C=O functional groups, respectively.[7] The O 1s spectrum in Figure S1 is deconvoluted into two peaks at 531.9 and 533.4 eV corresponding to C=O, and C–O functional groups.[7] The large oxygen and carbon-containing functional groups on the HAC surface could improve the electrochemical wettability and storage.

Electrochemical Characterization of HAC

HAC–Single Electrode Study

To understand the role of the carbon to KOH ratio in energy storage, preliminary cyclic voltammetry (CV) is carried out using a single-electrode supercapacitor in 2 M Na_2SO_4 with a potential window of 0 to −1 V. This technique (CV) is commonly used to screen the electrode materials and the voltage window of the aqueous electrolytes.[26] The preliminary CV curves as shown in Figure 5 of the HAC with different KOH ratios as activating agents. Both materials exhibit the characteristics of electric double-layer capacitors (EDLC),[27,28] while the ratio (1:2) demonstrates improved capacitance than the ratio (1:1). Under identical conditions, the ratio (1:2) has a current response much larger than that of the 1:1 electrode and to the area under the curve is directly proportional to the capacitance. The performance transition from 1:1 to 1:2 could be mainly attributed to the role of the morphology and pore size and shape in accessing the ion adsorption characteristics.[27–29] Although both have ascertained the charge storage mechanism with a capacitive signature, the improved ratio (1:2) has been chosen for further electrochemical studies.

Figure 6a shows the CV curves for the HAC at different scan rates. The quasi-rectangular shape of the CV curves, without any redox peak, is observed for low scan rates (5–40 mV/s) when the scan rate is progressively increased, there is a deviation from the quasi-rectangular shape resulting in distorted CV, which could be due to a higher degree of electrochemical polarization.[16] The efficient charge transfer rate on the electrode surface is observed in the hierarchical porous structure of carbon even at a high rate of 40 mV/s. The quasi-rectangular shape of the CV curves compares quite favorably to the reported work of some microporous carbon obtained from biomass and tested at lower scan rates.[7,30,31] Additionally, galvanostatic charge-discharge (CD) has been used to analyze the capacitive performance of the activated carbon. To assess the rate capabilities of the HAC, the charge-discharge cycling was measured at various specific currents from 1 to 20 A/g and the CD profiles are plotted in Figure 6b and Figure S3. The material demonstrates 360, 240, 180, 150, 135, and 120 F/g at the specific current densities of 1, 2, 5, 10, 15, and 20 A/g, respectively. The CD profile for the lower specific current densities (1 $A g^{-1}$) is compared and shown in Figure S3. The specific capacitance values are calculated using Equation (2) and the obtained values are quite comparable to that of the reported.

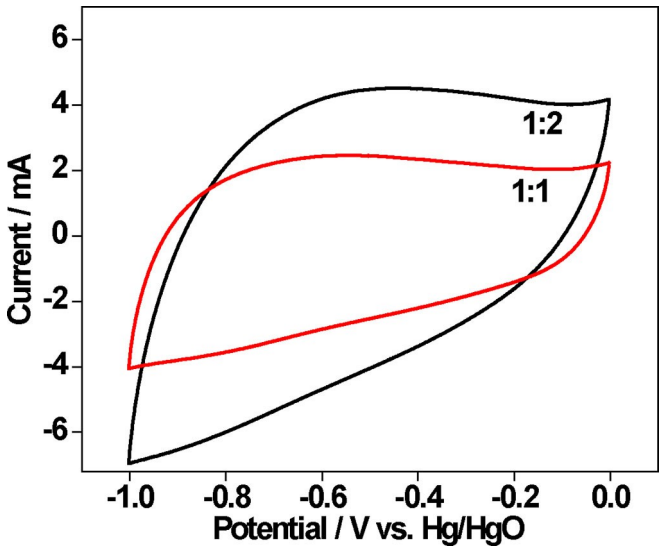

Figure 5. Preliminary Cyclic Voltammogram (CV) to assess the suitability of HAC electrodes synthesized at various impregnation ratios. The hemp-derived biochar to KOH ratio in the HAC electrode is shown in the diagram. The ratio 1:2 exhibits a larger peak showing a typical capacitive curve.

value for biomass-based supercapacitors and higher than that for commercial activated carbon (105 F/g).[32] The CV profile at lower scan rates (2–20 $A g^{-1}$) showed (in Figure S4) both characteristics of capacitive and pseudocapacitive (faradaic non-diffusion limited) charge storage while at higher scan rates >20 $A g^{-1}$ the contribution from capacitive storage dominates. The charge storage contribution was analyzed using the CV data by the power law method $i = av^b$ where a and b are constants, i is the measured current (mA), ν is the scan rate (V s^{-1}).[33] The obtained b-value 1 indicates capacitive and pseudocapacitive behavior are observed. The studied HAC material exhibits the quasi-rectangular shape of the CV curve, however, the mass transport is negligible, depending on the scan rate. The charge-discharge curves shown in Figure 6b are almost linear with a symmetrical triangular shape exhibiting capacitive behavior with a very small and fast potential (IR) drop initially, suggesting that the carbon material is highly conductive and porous texture. This is also further confirmed by the electrochemical impedance spectroscopy results shown in Figure 6c. At high frequencies (Figure 6c; inset) the plot was characterized by a distorted semicircle followed by an inclined 45° capacitive line, which is a characteristic behavior of porous carbon electrodes reported for supercapacitors.[34] It is to be noted that the equivalent series resistance (ESR) value is as low as 0.9 Ω, obtained from the extrapolation on the real axis intercept of the Nyquist pot in Figure 6c. This is attributed to the right balance of the graphitic and disordered structure of the ratio (1:2) HAC activated at mild 450 °C. The cycling stability and capacitance retention are critical factors for the supercapacitors in application. HAC has been cycled at 10 A/g to evaluate its cycling stability in a single-cell, three-electrode configuration. A reversible capacitance of 144 F/g displaying 98.3 % capacitance retention after 15,000 cycles indicates the material qualifies to be a negative electrode in an asymmetric supercapacitor.

However, before exploring asymmetric studies, we attempted to test HAC in the positive region and built a symmetric (HAC vs. HAC) cell. The results are shown in Figure 7. The single-electrode supercapacitor in 2 M Na_2SO_4 with a potential window of 0 to 0.6 V shows a redox behavior, which is quasi-reversible, and is devoted to the insertion of sodium/OH− ions from the electrolyte.[27,29] However, the current response is significantly low (compare y-axes in Figures 6a and 7a). This is further justified in Figure 7b by comparing the magnitude of

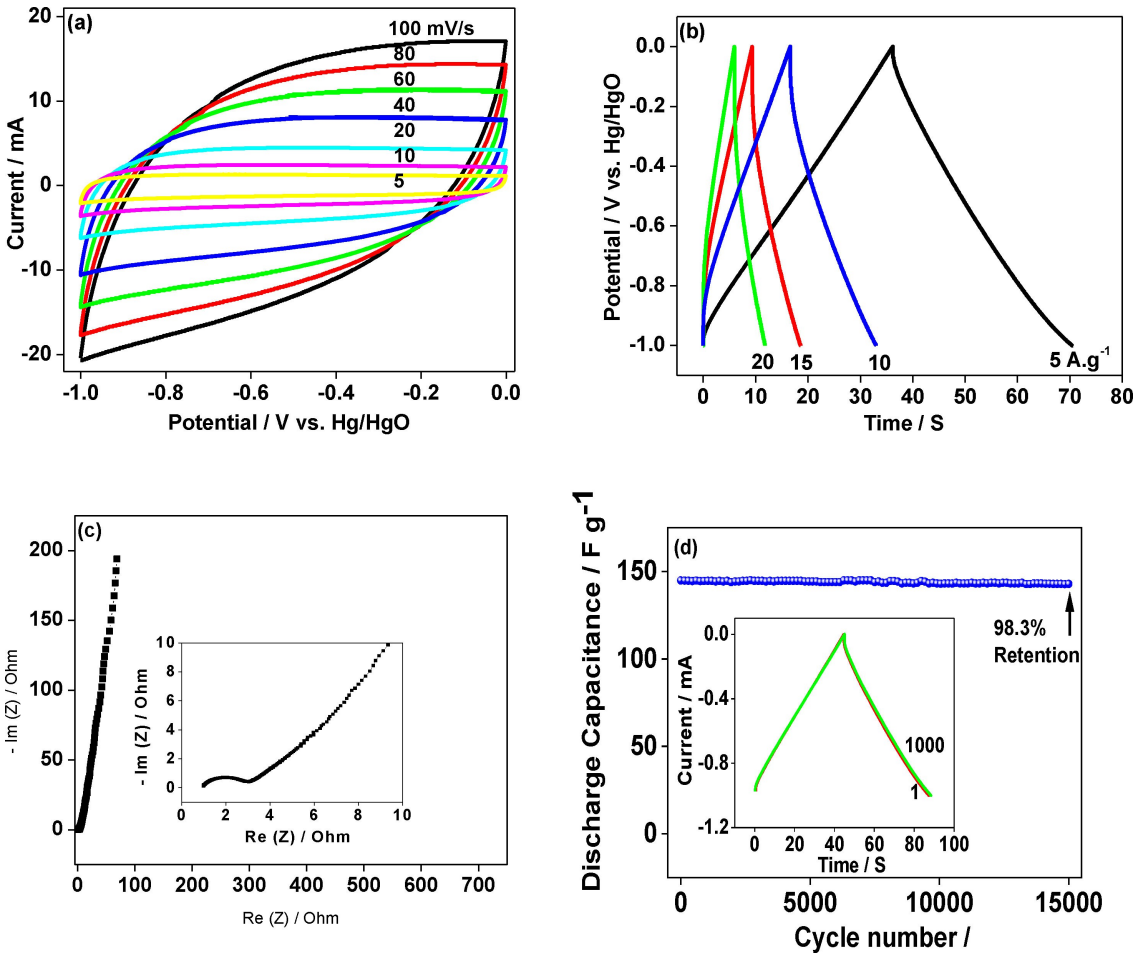

Figure 6. Electrochemical behavior of HAC single electrode. (a) CV curves of HAC at different scan rates; (b) GCD curves of HAC at different current densities; (d) Nyquist plot for HAC and the inset showing the enlarged image of the high-frequency region. Cycle stability of the electrode was recorded at a current density of 10 A/g showing the specific capacitance retention for 15000 cycles. The scan rates and current rates are indicated in the respective panels.

the HAC curves covering the entire (positive and negative) regions. The charge storage mechanisms in the negative and positive regions correspond to EDLC (supercapacitor), and redox (battery) behavior, involving non-faradic and faradic charges, respectively. This finding suggests that the morphological characteristics of the hierarchical pores contributed to effective ion diffusion resulting in a faradaic charge transfer in the positive region. By coupling the two similar HAC electrodes, we built a device, and the CV response is shown in Figure 7c. It can be seen that the shape of the curves and the current response are not prominent for any applications. This suggests that HAC is a state-of-the-art negative electrode and not suitable for positive regions.

Hence, alternatively, we have identified electrolytic manganese dioxide (EMD) to couple with HAC in an asymmetric cell, and the preliminary CV plots are shown in Figure 7d. The electrochemical properties of EMD are described in one of our earlier reports.[35] The HAC supercapacitor (EDLC) electrode is shown in the negative region while the EMD electrode shows a pseudocapacitor behavior in the positive region with a similar current response but at different mass loadings (as detailed in the methodology section). The HAC electrode corresponds to 240 F/g while the EMD corresponds to 95 F/g and based on this storage performance, the mass loadings are optimized for asymmetric devices as stated in Equation (1).

Hybrid Device HAC vs. EMD

Then, we fabricated a hybrid device (asymmetric cell) with two dissimilar materials as shown in Figure 8. The device was tested in a Hohsen electrochemical cell. To assess the maximum operating voltage of the hybrid device comprising HAC *vs.* EMD, CV was performed at a scan rate of 50 mV/s. Figure 8a presents the CV profile for various supercapacitor voltages, as seen in this figure, the shape of the CV remains constant implying there is no distortion in the curve and all the curves are fully reversible. The voltage window widening experiments on an asymmetric supercapacitor show an operating voltage of 2 V for the device seems suitable in neutral electrolyte. Figure 8b shows the CV profile for the device with a potential window of 2 V, where a quasi-rectangular shape is reasonably maintained for all the curves (5–100 mV/s), and the current response is progressively increased. The hybrid device exhibits

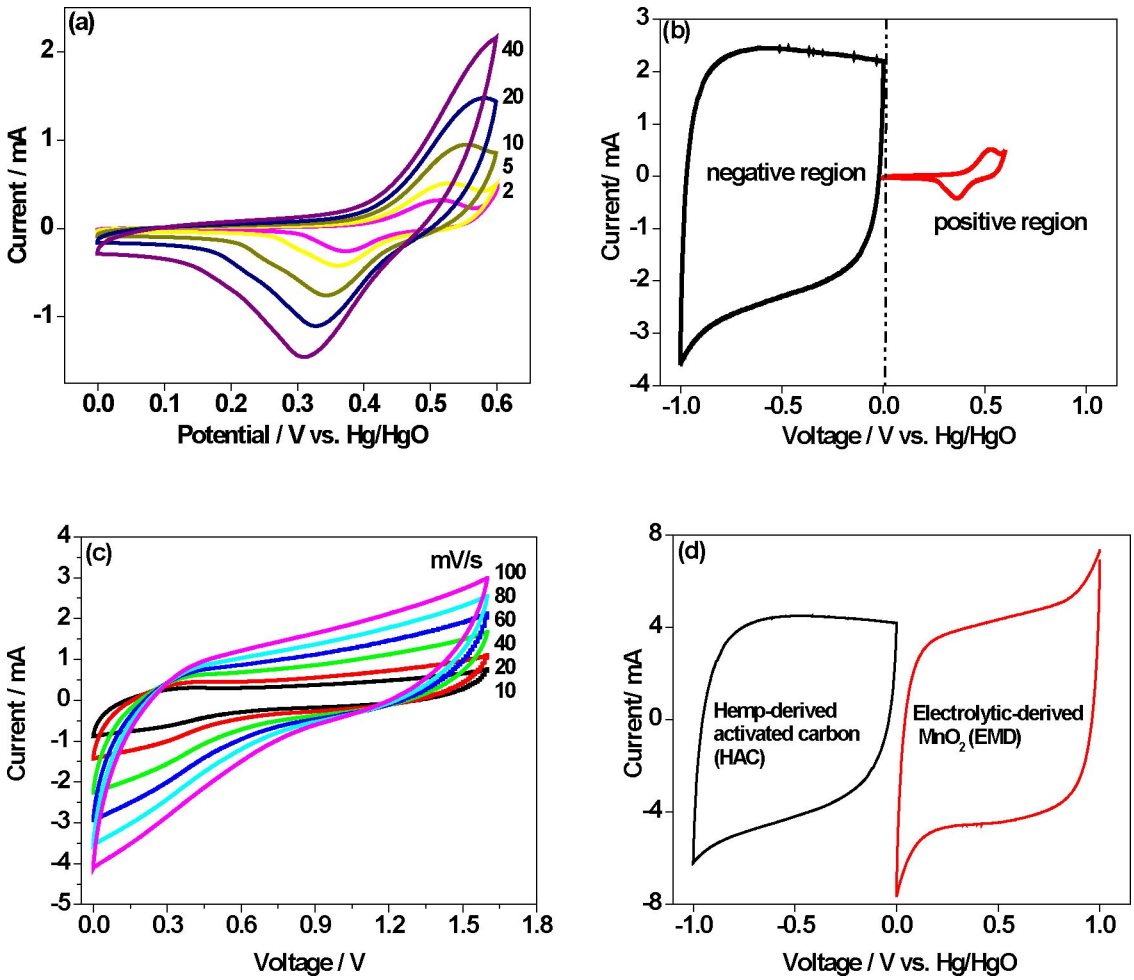

Figure 7. Electrochemical behavior of HAC symmetric electrode configuration. (a) CV curves of HAC in the positive region at different scan rates; (b) CV curves of HAC in both negative and positive regions, implying the potential of HAC is superior in the negative region; (c) CV curves of HAC||HAC symmetric cell in 1.8 V window at different scan rates; and (d) CV curves of HAC in the negative, and EMD in the positive region. The scan rates and current rates are indicated in the respective panels.

a pseudocapacitive behavior, and also the charge-discharge curves in Figure 8c exhibit a sloped discharge curve with an inflection suggesting an intermediate behavior (neither related to a capacitor having a triangular shape nor a battery related to a flat discharge plateau).[36] The observed negligible IR drop even at higher current rates suggests that both the materials in the hybrid devices have good electrical conductivities and porous structures. The hybrid device demonstrates 75, 50, 40, and 30 F/g at the specific current densities of 1, 2, 4 and 8 A/g, respectively. The electrode capacitance contribution is from the adsorption and desorption of ions (EDLC) and the Na/SO_4 ions diffusion to the EMD electrode. The underlying storage mechanisms and the electrochemical processes occurring during the charge-discharge storage in this work are similar to the principles explained in the literature.[35] The obtained capacitance values are quite comparable to that of the reported value for biomass-based hybrid device supercapacitors and are related to pseudocapacitive redox reactions.[7,13,16,19,33,34] This is attributed to the observed specific area of the samples, and the chosen sodium electrolyte rather than the surface functional groups, as the irreversibility and rate capability are stable. The device shows a Nyquist plot, in Figure 8d, typical for supercapacitors, having main features such as distorted semicircle at high frequencies due to contact resistance among the particles, and a slope at medium frequencies indicating a pore resistance. The distorted semicircle with lower resistance in Figure 8d also indicates the access of the electrolyte ions in the pores of the material. The multiple charge-discharge cycling at 0.5 A/g in 0–2 V has been used to determine long-term cycling stability. The long-term cycling along with the charge-discharge curves (in the inset) superimposed for 1, 500, and 1000 cycles are shown in Figure 8e. An initial specific capacitance of 105 F/g was achieved for the device, which dropped to a value of 95 F/g after 1000 cycles with a retention of 91 %. The capacitance was dropped for the first 400 cycles and thereon it stabilized. The shape of the charge-discharge curves is consistent showing the charge storage is reversible. Thus, the reported hybrid device has good storage, which is attributed to the morphology and large surface area, and can be an alternative to the AC materials derived at a high temperature. The energy and power densities

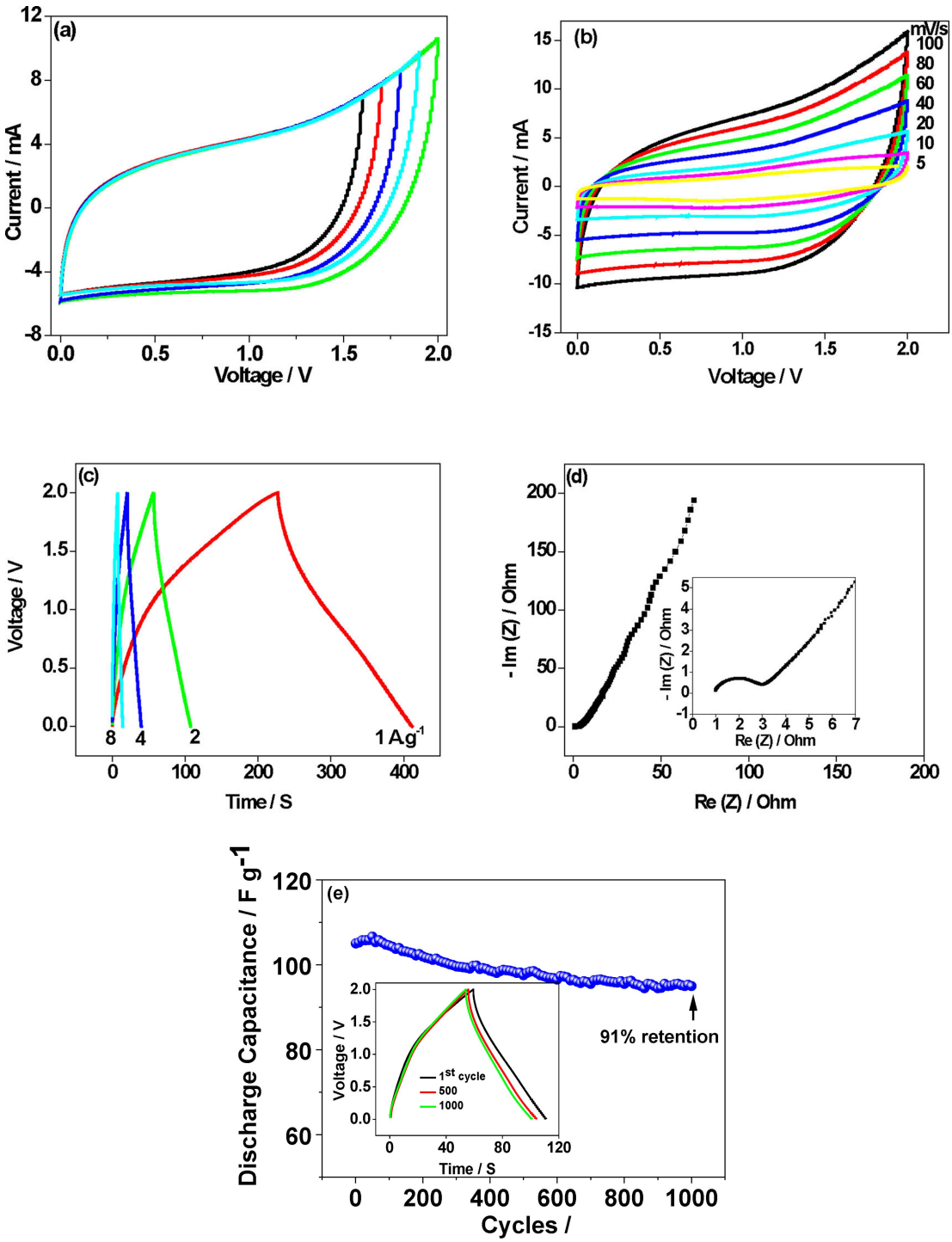

Figure 8. Electrochemical behavior of the asymmetric cell (ASC) HAC||EMD device. (a) CV curves of the device at different voltage windows displaying 2 V profile; (b) CV curves of the device at different scan rates; (b) GCD curves of the device at different current densities; (d) Nyquist plot for HAC and the inset showing the enlarged image of the high-frequency region. (e) The cycle stability of the electrode shows the specific capacitance retention. The inset of Figure 8e shows the superimposed CD curves for the multiple cycles implying the reversibility. The scan rates and current rates are indicated in the respective panels.

are calculated using Equations (3) and (4). Figure 9 shows Ragone plots of our HAC hybrid device, which delivers a specific energy (calculated using Equation (5) in Section 2) from 139 to 61 Wh/kg as the specific power is increased from 2.7 to 27 kW/kg. Figure 9 (inset) also compares the energy-power characteristics of our hybrid device with reported similar hemp and biomass-derived activated carbon for asymmetric supercapacitors.[7,13,16,19,33,34] It can be seen from the inset that our device is competitive as the energy density is higher for a specific power density than that reported in the literature.

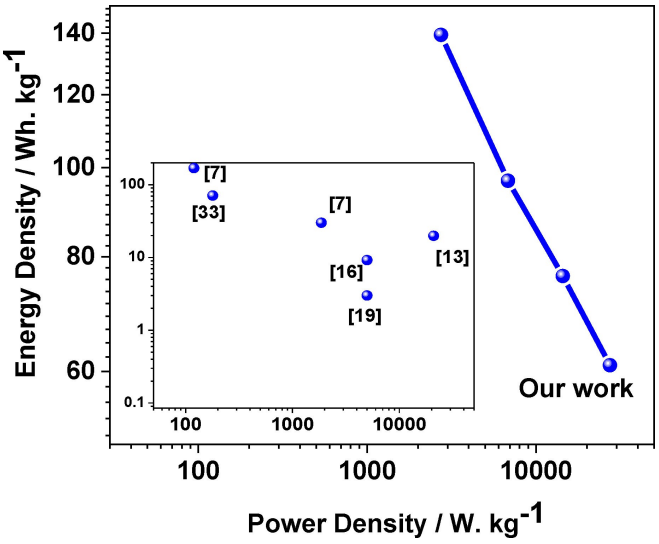

Figure 9. Ragone plot of HAC | | EMD-based asymmetric supercapacitor (ASC). The values are benchmarked in the inset with the relevant biomass-derived AC reported in the literature.

Therefore, practically, the activated carbons derived from biomass hemp as a precursor via mild synthesis can be used to prepare the electrodes that power aqueous supercapacitors. This could replace expensive carbonaceous materials allowing us to economically produce HAC on a large scale effectively.

Conclusions

To summarise, the findings of the present study indicate that hard carbon produced from waste hemp via mild chemical activation with KOH at 450 °C exhibits remarkable electrochemical performance as an anode in hybrid supercapacitors. The biomass hemp powder activated with melted KOH solution plays both a deoxidant and activating agent by skipping the requirement of high temperature that led to molecular level activation of hemp in subsequent one-step calcination at 450 °C. The 3D honeycomb structure of HAC resulted in a very high surface area with lower surface functional groups on the surface resulting in a high specific capacitance of 240 F/g at 1 A/g and found to be highly reversible with an excellent retention rate of 98%. The obtained pore sizes are most effective in a double-layer formation, which correlates well with the size of hydrated ions. The work provided insights into the impregnation ratio and the activation temperature which is translated into an interconnected porosity, optimized amount of structural defects, and compact porous deposits that can explain the observed improved capacitance without much IR drop. The asymmetric (hybrid) capacitor (HAC | | EMD) of 2 V in aqueous 2 M Na_2SO_4 electrolyte exhibited a specific capacitance of 105 F/g having a high energy density of 38 Wh/kg at a power density of 761 W/kg. The long-term cycling stability at 1 A/g provided a capacitance retention of 91% after 1000 cycles. This hybrid device not only delivers fast aqueous supercapacitors but also high energy density.

Experimental

Synthesis of HAC

Hemp Biochar: Mechanically decorticated waste hemp hurd sticks (*Cannabis sativa L.)* were provided by the Food, Fibre and Land International (FFLI) group and MIRRECO Products Ltd. The sticks were rinsed under running deionised water (DI) water at 20 °C to remove impurities and dried in the oven at 50 °C for 2 h before use. Then the dried long fiber structures of the hemp hurd sample were ground into small lumps of size approximately 6–8 mm and kept in a dry atmosphere at room temperature. In the current work, an alternative synthesis approach has been taken to synthesize activated carbon using hemp as the precursor (termed hemp-derived activated carbon - HAC), which uses scalable and conventional heating methods rather than advanced methods such as producing hydrochar under controlled pressure in the presence of inert gas. The ground hemp sample was carbonized in a conventional furnace under 300 °C for 2 h at an ambient atmosphere, and allowed to cool at room temperature. The obtained biochar is safely secured in airtight storage at room temperature. It is observed that biochar yield under the same operating conditions with an open lid would produce a yield of 21%, while a covered lid produced a yield of 38%. This is mainly due to the lid preventing any biochar from escaping into the furnace environment under ambient atmospheric conditions.

Chemical Activation of Hemp: The obtained carbonized sample (biochar) was chemically activated with potassium hydroxide (KOH) as the activating reagent. The melting point for KOH is around 400 °C range, where it is converted from KOH into K_2CO_3, which is later evaporated at further higher temperatures ranging from 750 °C and above. To understand the role of activating agents and temperature in the electrochemical properties, the ratio of biochar (carbon) to KOH, and the activating temperature have been examined. The appropriate amounts of hemp fiber-derived biochar to KOH (1 : 1 or 1 : 2) are mixed in the mortar using pestle into finer lumps. Then, the mixture is dried at 90 °C for 24 h to dehydrate any surface moisture. Finally, the apportioned each mixture is heated at 450 and 800 °C for 1 h and cooled to room temperature. The excess KOH base in the activated carbon and other unreacted K_2CO_3 was neutralized by acid treatment with 1 M HCl (32%) followed by washing with DI until pH was neutral ≈7. Then, the HAC sample was dried in the oven at 60 °C for 12 h.

Physical Characterization of HAC

The structural determination of the synthesized HAC samples for different biochar to KOH ratios (1 : 1, and 1 : 2) and synthesis temperatures 450 °C and 800 °C was carried out by X-ray diffraction (Rigaku, Japan) using Cu Kα radiation. The Fourier-transform infrared (FT-IR) using NICOLET iS20 instrument (Thermo-Fisher Scientific, Waltham, MA, USA), and Raman Spectroscopy using an NRS-3100 (JASCO, Tokyo, Japan) instrument at the excitation wavelength of neon laser 532.09 nm were used for identifying the surface functional groups and nature of carbon present in the bulk and surface of the samples. Each sample was analyzed on at least three different surface locations at a depth of 3 μm. The morphology and elemental composition on the surface of the synthesized HAC were analyzed using Field Emission Scanning Electron Microscopy (FESEM, TESCAN CLARA). Transmission electron microscopy (TEM) images were collected using a JEOL 2200FS TEM operated at 200 kV. TEM specimens were prepared by grinding a small amount of hemp sample powder under ethanol in an agate mortar and pestle and dispensing via pipette onto a holey carbon film supported on a TEM copper mesh grid. Elemental maps were

collected in scanning TEM (STEM) mode via X-ray energy dispersive spectroscopy (EDS) using an Oxford X–Max 80 mm^2 detector interfaced with Oxford INCA, version 4.15, microanalysis software. Surface area and pore analysis (SAPA) of the samples were carried out by N_2 adsorption-desorption isotherms at 77 K. The obtained specific surface area was calculated by the Brunauer-Emmett-Teller (BET) method.

Electrochemical Characterization of HAC

For electrochemical measurement, the electrode was prepared by mixing either HAC or Electrolytic Manganese Dioxide (EMD) (75 wt%), carbon black (15 wt%), and polyvinylidene difluoride PVDF (10 wt%) with 0.4 mL of N-Methyl-2-pyrrolidone (NMP) to make a slurry. This was coated on a small piece of graphite sheet (area of coating, 1 cm^2). The loaded active material was around 2 mg in each case. For the three-electrode tests, a platinum wire of 10 cm length and 1 mm diameter in dimension and mercury-mercuric oxide (Hg/HgO) served as the counter and reference electrodes, respectively. In single-electrode tests, HAC served as the working electrode. An asymmetric cell (ASC) full cell termed a "hybrid device" (HAC||EMD) was fabricated by using Whatman filter paper as a separator, where the separators are wetted nicely with the electrolyte. The cyclic voltammetry and galvanostatic charge-discharge studies of the composites were carried out using SP-150, Bio-Logic Science instruments in 2 M Na_2SO_4 electrolyte at room temperature. For HAC, the working electrode was cycled between 0 and −1.0 V while for the hybrid device, the cell was tested at varying voltage windows and optimized at 2 V. For the asymmetric cell, measurements were performed in an Hohsen electrochemical cell. For a hybrid device, to maintain the charge conservation between the two electrodes, the mass ratio was also calculated using Equation (1). The mass balancing of the positive (EMD) and negative electrodes (HAC) was carried out using Equation (1).

$$m_+/m_- = (C_- \times \Delta V_-)/(C_+ \times \Delta V_+) \quad (1)$$

where m_+ and m_- are effective masses (g), C_+ and C_- are the capacitance of active material (F/g), and ΔV^+ and ΔV^- are the working potentials (V) of the positive and negative electrodes respectively. The specific capacitance was computed from the following Equation (2).

$$C_s = \frac{I\,t}{m\,\Delta V}\ (F/g) \quad (2)$$

where C_s is the specific capacitance in (F/g), I is current in (mA), $\triangle t$ is the discharging time (s), m is the mass of the active material loaded (mg) and ΔV is the potential window (V). The specific capacitance of the HAC and EMD were calculated to be 240 F/g and 95 F/g. Therefore, for a mass of 1 mg of HAC, the mass of the EMD was 2.5 mg. The energy and power density of the device was calculated using the formulas (3–4)

$$E = \frac{1}{2} \times \frac{1}{3.6} \times CV^2(Wh/kg) \quad (3)$$

$$P = \frac{E \times 3600}{t}\ (W/kg) \quad (4)$$

where E and P denote the energy density (Wh/Kg) and power density (W/Kg) of the device, C is the estimated specific capacitance (F/g). However, for benchmarking the performance metrics in the Ragone plot, to be on par with the reported values in the literature, Equation (3) has been modified to the following Equation (5).

$$E = \frac{1}{2} CV^2(Wh/kg) \quad (5)$$

Acknowledgements

M. M. acknowledges the Winston Churchill Fellowship to learn globally and inspire locally. This work was partially supported by the Japan Society for the Promotion of Science (JSPS) KAKENHI Grant Numbers JP20H00392 and JP23H05459. Open Access publishing facilitated by Murdoch University, as part of the Wiley - Murdoch University agreement via the Council of Australian University Librarians.

Conflict of Interests

The authors declare no conflict of interest.

Data Availability Statement

The data that support the findings of this study are available from the corresponding author upon reasonable request.

Keywords: Biomass · Carbon · Energy storage hemp · Hybrid capacitor

[1] A. S. Mohd Razif, N. F. Ab Aziz, M. Z. A. Ab Kadir, K. Kamil, *Energy Strategy Rev.* **2024**, *52*, 101346.
[2] Y. Chen, Y. Kong, Y. Zhao, L. Wang, J. Liu, Y. Li, Z. Liang, X. He, X. Li, N. Tavajah, B. Li, *J. Energy Chem.* **2021**, *59*, 83–89.
[3] S. Chen, M. Zhang, P. Zou, B. Sun, S. Tao, *Energy Environ. Sci.* **2022**, *15*, 1805–1839.
[4] X. Liu, Y. Sun, Y. Tong, X. Wang, J. Zheng, Y. Wu, H. Li, L. Niu, Y. Hou, *Nano Energy* **2021**, *86*, 106070.
[5] L. L. Zhang, X. S. Zhao, *Chem. Soc. Rev.* **2009**, *38*, 2520–2531.
[6] D. Antoran, D. Alvira, M. Eser Peker, H. Malon, S. Irusta, V. Sebastian, J. Manya, *Energy Fuels* **2023**, *37*, 9650–9661.
[7] J. Chen, X. Zhou, C. Mei, J. Xu, S. Zhou, C. P. Wang, *J. Power Sources* **2017**, *342*, 48–55.
[8] Z. Ding, V. Trouillet, S. Doske, *J. Electrochem. Soc.* **2019**, *166*, A1004–A1014.
[9] M. Gayatri, T. Pulingam, K. T. Lee, K. Sudesh, *Chemosphere* **2022**, *294*, 133764.
[10] G. G. Stavropoulos, A. A. Zabaniotou, *Fuel Process. Technol.* **2009**, *90*, 952–957.
[11] H. Wang, Z. Xu, A. Kohandehghan, Z. Li, K. Cui, X. Tan, T. J. Stephenson, C. K. King'ondu, C. M. B. Holt, B. C. Olsen, J. K. Tak, D. Harfield, A. O. Anyia, D. Mitlin, *ACS Nano* **2013**, *7*, 5131–5141.
[12] M. Sarker, C. Wan, *Ch. 8 Adv. Bioenergy* **2022**, *7*, 343–366.
[13] W. Sun, S. M. Lipka, C. Swartz, D. Williams, F. Yang, *Carbon* **2016**, *103*, 181–192.
[14] R. Yang, G. Liu, X. Xu, M. Li, J. Zhang, X. Hao, *Biomass Bioenergy* **2021**, *35*, 437–445.
[15] S. M. Lee, S. H. Lee, J. S. Roh, *Crystals* **2021**, *11*, 153.
[16] J. Cheng, Q. Xu, X. Wang, Z. Li, F. Wu, J. Shao, H. Xie, *Sustain. Energy Fuels* **2019**, *3*, 1215–1224.
[17] R. Vali, A. Janes, T. Thomberg, E. Lust, *Electrochim. Acta* **2017**, *253*, 536–544.
[18] J. Dorado, G. Almendros, J. A. Field, R. S-Alvarez, *Enzyme Microb. Technol.* **2001**, *28*, 550–559.

[19] Z. Zhang, W. Yang, Y. Wu, G. Yan, L. Li, Y. Qing, X. Lu, *Ind. Eng. Chem. Res.* **2021**, *60*, 11079–11085.
[20] Y. Zhang, A. N Md. Ahsanul Haque, M. Naebe, *Nanomaterials* **2021**, *11*, 3425.
[21] N. Stevulova, J. Cigasova, A. Estokova, E. Terpakova, A. Gelfert, F. Kacik, E. Singovszka, M. Holub, *Materials (Basel)* **2014**, *7*, 8131–8150.
[22] G. Balciunos, S. Vejelis, S. Vaitkus, A. Kairyte, *Procedia Eng.* **2013**, *57*, 159–166.
[23] Y. Jiang, M. Lawrence, M. P. Ansell, A. Hussain, *R. Soc. Open Sci.* **2018**, *5*, 171945.
[24] P. Chaowana, W. Hnoocham, S. Chaiprapat, P. Yimlamai, K. Chitbanyong, K. Wanitpinyo, T. Chaisan, Y. Paopun, S. Pisutpiched, S. Khantayanuwong, B. Puangsin, *Mater. Sci. Energy Technol.* **2024**, *7*, 19–28.
[25] V. Gomez-Serrano, C. M. Gonzalez-Garcia, M. L. Gonzalez-Martin, *Powder Technol.* **2001**, *116*, 103–108.
[26] N. Elgrishi, K. J. Rountree, B. D. McCarthy, E. S. Rountree, T. E. Eisenhart, J. L. Dempsey, *J. Chem. Educ.* **2018**, *95*, 197–206.
[27] T. Brousse, D. Belanger, J. W. Long, *J. Electrochem. Soc.* **2015**, *162*, A5185–A5189.
[28] S. Deebansok, J. Deng, E. Le Calvez, Y. Zhu, O. Crosnier, T. Brousse, O. Fontaine, *Nat. Commun.* **2024**, *15*, 1133.
[29] V. Sawant, R. Deshmukh, C. Awati, *J. Energy Chem.* **2023**, *77*, 438–451.
[30] Y. Li, D. Zhang, Y. Zhang, J. He, Y. Wang, K. Wang, Y. Xu, H. Li, Y. Wang, *J. Power Sources* **2020**, *448*, 227396.
[31] Z. Bi, Q. Kong, Y. Cao, G. Sun, F. Su, X. Wei, X. Li, A. Ahmad, L. Xie, C. M. Chen, *J. Mater. Chem. A* **2019**, *27*, 16028–16045.
[32] F. Cheng, W. Qiu, X. Yang, X. Gu, W. Hou, W. Lu, *Electrochim. Acta* **2022**, *403*, 139728.
[33] H. Lindstrom, S. Sodrgren, A. Solbrand, H. Rensmo, J. Hjelm, A. Hagfeldt, S. E. Lindquist, *J. Phys. Chem. B.* **1997**, *101*, 7717–7722.
[34] J. Li, Y. Gao, K. Han, J. Qi, M. Li, Z. Teng, *Sci. Rep.* **2019**, *9*, 17270.
[35] K. Wickramaarachchi, M. Minakshi, *J. Energy Storage* **2022**, *56*, 106099.
[36] J. Liu, J. Wang, C. Xu, H. Jiang, C. Li, L. Zhang, J. Lin, Z. X. Shen, *Adv. Sci.* **2018**, *5*, 1700322.

Manuscript received: June 12, 2024
Revised manuscript received: August 12, 2024
Accepted manuscript online: August 28, 2024
Version of record online: October 23, 2024